Microfluidic Printheads for Multimaterial 3D Printing of Viscoelastic Inks

*James O. Hardin, Thomas J. Ober, Alexander D. Valentine, and Jennifer A. Lewis**

The ability to integrate both form and function within printed objects is the next frontier in 3D printing. To move beyond prototyping, new materials and flexible printing platforms are required. One promising method, known as direct ink writing, utilizes viscoelastic inks composed of myriad materials, including ceramic particles,[1,2] metal particles,[3,4] polyelectrolytes,[5] hydrogels,[6,7] filled epoxy resins,[8] and even cell-laden extracellular matrices.[9] To date, this extrusion-based printing method has been used to fabricate functional devices (e.g., 3D antennas,[4] rechargeable microbatteries,[2] wearable sensors,[10] structural composites,[8] and vascularized 3D tissue[9]). This printing approach has also been utilized for high-throughput printing,[11] and also for architectures incorporating multiple materials;[9,12] however, the construction of multimaterial architectures often involves sequentially printing individual materials using multiple nozzles. The drawbacks of printing one material at a time include the need to carefully align each nozzle as well as start-and-stop ink flow on demand without introducing defects.

Here, we demonstrate multimaterial 3D printing using a microfluidic printhead specifically designed for seamlessly switching between two viscoelastic materials "on-the-fly" during fabrication. To demonstrate these capabilities, model viscoelastic inks based on polydimethylsiloxane (PDMS) elastomers of varying composition are printed in 1D, 2D, and 3D architectures. An analytical model is developed to determine the relationships between the ink rheology, printing parameters (i.e., applied pressure and printing speed), and printed filament composition. The ability to print multiple materials from the same nozzle in a programmable manner opens new opportunities for creating functional matter with encoded compositional and property gradients defined solely by print path.[13,14]

Five PDMS inks (**Table 1**) were formulated using a combination of 2-part SE 1700 (Dow Corning), anhydrous hexanes (95% purity, Sigma–Aldrich), and silicone oil (Thermo Fisher Scientific). Red Silc Pig silicone pigment (Smooth-On) and CdSeS/ZnS 6 nm quantum dots (QD) with emission peaks at either 490 or 630 nm (Sigma–Aldrich) were added as color modifiers. The ratio of base and catalyst was varied for certain inks to affect the compliance of the printed structure after curing. The rheological behavior of the PDMS inks under steady shear and oscillatory shear is shown in **Figure 1** and Figure S1, Supporting Information, respectively. This ink exhibited a shear thinning response with an apparent viscosity of $\eta = 91$ Pa s at a shear rate of $\dot{\gamma} = 10\ s^{-1}$ and a shear yield stress of $\tau_Y = 550$ Pa. The ink is well described by the Herschel–Bulkley (HB) model:[15]

$$\tau = \eta(\dot{\gamma})\dot{\gamma} = \tau_Y + K\dot{\gamma}^n \quad (1)$$

where $K = 80$ Pa $s^{0.65}$ is the consistency index, and $n = 0.65$ is the power-law exponent.

To simultaneously print multiple viscoelastic inks through a single nozzle, we custom-designed and fabricated a microfluidic printhead shown schematically in **Figure 2**a. During printing, the nozzle is stationary and the substrate is translated using a 3-axis, motion-controlled gantry. Two opposed syringe pumps alternately push the inks through two square channels ($h = w = 200$ μm) with hydraulic diameter $d_1 = 200$ μm and an approximate length $l_1 = 1000$ μm, and into a microfluidic junction at the bottom of the nozzle (Figure 2b,c). The junction and final expansion section have diameters $d_2 = 200$ μm and $d_3 = 400$ μm, respectively, and their lengths are $l_2 = l_3 = 200$ μm. The small size of the junction reduces the transition volume of the nozzle, taken as $V_T \approx \frac{\pi}{4} d_2^2 (h + l_2) = 12.6$ nL, and thereby expedites the switching process. The expansion is included to sharpen the transition between different materials in the printed filaments (**Figure 3**a), for which the minimum estimated transition length is $L_T = \frac{4}{\pi} V_T / d_3^2 = 100$ μm. The small dimensions of the junction region also mitigate the growth of interfacial instabilities between the materials,[16] which would have otherwise adversely affected the transition sharpness.

We used volumetric-controlled flow to precisely dispense the desired volume of ink through the printhead. A typical pumping protocol of set flow rates and corresponding pressures is provided in Figure 3b. During steady printing of one ink (A) over time t_s, the pumping flow rate on syringe A is $Q_{p,A} = Q_s$, while $Q_{p,B} = 0$ for the other ink (B). The corresponding pressures in the syringes are $P_A = P_s$ and $P_B = P_m$. To generate the desired switching transition between the two inks (Movie S1, Supporting Information), the pressures in syringes A and B must fall and rise, respectively, by $\Delta P_p = P_s - P_m$ within a fixed period of time t_p. To expedite this pressure change, an infusion pulse $Q_{p,B} = Q_p$ on syringe B and a withdrawal pulse $Q_{p,A} = -Q_w$ on syringe A are simultaneously applied to rapidly compress and decompress the inks in each syringe. After this pulsing period, steady printing rates are resumed with $Q_{p,A} = 0$ and $Q_{p,B} = Q_s$. The process is reversed to switch back from ink B to A.

Dr. J. O. Hardin, Dr. T. J. Ober, A. D. Valentine, Prof. J. A. Lewis
Harvard School of Engineering and Applied Sciences
Wyss Institute for Biologically Inspired Engineering
Cambridge, MA 02138, USA
E-mail: jalewis@seas.harvard.edu

DOI: 10.1002/adma.201500222

ADVANCED MATERIALS
www.advmat.de

www.MaterialsViews.com

Table 1. Elastomer ink formulations given in weight percentages.

Ink	PDMS base	PDMS catalyst	Silicone oil	Red pigment	Red QD	Green QD	Hexane
A	83.0	0	16.6	0	0.4	0	0
B	83.0	0	16.6	0	0	0.4	0
C	78.6	7.8	0	3.6	0	0	10
D	81.8	8.2	0	0	0	0	10
E	87.1	2.9	0	0	0	0	10

Unfortunately, system compressibility can cause significant transient periods in microfluidic printheads as pressures adjust to sudden changes in imposed flow rates,[17] which can severely attenuate the sharpness of the transition between different inks (Figure 3c). To develop a framework to qualitatively understand the effects, we model the printhead (Figure 3d) as a combination of connected syringes (capacitors) and microchannels (resistors) with flow rates (current) that instantaneously adjust to the pressure drops (voltage) according to the HB model (see the Experimental Section). For the model to be applicable, we must further assume the pumps reliably and accurately achieve the set flow rates and they start and stop instantaneously, and the effects of compressibility can be described by a constant isothermal compressibility coefficient $\beta \equiv -\frac{1}{V}\left(\frac{\partial V}{\partial P}\right)_T$ of the system, where $V = V_A = V_B$ is the net ink volume in each syringe. To achieve a steady flow rate through the nozzle outlet, it is necessary to maintain a constant pressure within the junction $P_J = P^* = P_0 + \Delta P_2(Q_s)$, where $\Delta P_2(Q_s)$ is the pressure drop from the junction to the outlet at Q_s. Hence, $P_s = P^* + \Delta P_1(Q_s)$, where $\Delta P_1(Q_s)$ is the pressure drop over the upstream channel between the syringe and the junction region. The minimum syringe pressure over the printing cycle is $P_m = P^* + \Delta P_Y$, where $\Delta P_Y = 4\frac{l_1}{d_1}\tau_Y$ is the minimum pressure drop below which the yield stress of the material is sufficient to prevent any appreciable flow from the syringe into the junction region. Accordingly, it can be shown that the necessary pulse and withdrawal values to achieve full transition between materials during the pulsing step were (see the Experimental Section and the Supporting Information):

$$Q_{p,FT} \approx Q_{w,FT} + Q_s \approx \frac{V}{t_p}\beta\Delta P_p \quad (2)$$

Hence, to attain low variations in the filament diameter the ideal withdrawal flow rate is $Q_{w,FT} = Q_{p,FT} - Q_s$. Consequently, for all printed structures the value of the withdrawal pulse is selected so that $Q_w = Q_p - Q_s$.

To evaluate the ability to seamlessly transition between viscoelastic inks, we printed two model inks composed of PDMS dyed with different fluorescent QDs (formulations A-B) at a constant gap height of 400 μm and print speed of 2.65 mm s^{-1} (Q_S = 20 μL min^{-1}) over a controlled range of pulse strengths, 200 < Q_P < 2000 μL min^{-1}. The spatial distribution of each ink along the printed filament is determined using confocal microscopy coupled with image analysis. The transition length equals the distance along the filament over which the fraction of red ink F_A varies from 80% and 20%. A representative printed filament (Q_P = 1600 μL min^{-1}) is shown alongside color intensity profiles obtained from different pulse strengths investigated in **Figure 4**a,b. Confocal images of all the printed filaments are provided in Figure S2, Supporting Information.

For pulse values below Q_P < 600 μL min^{-1}, the transition was too weak to determine a transition length according to our stated metric. For higher pulse values (600 < Q_P < 1200 μL min^{-1}), the compression in the syringes was large enough to generate syringe pressures to drive transitions greater than 60%, with transition length monotonically decreasing with Q_p. These cases represented partial transition of the interface between the materials across the outlet of the nozzle. The minimum pulse value for full transition was $Q_{P,FT}$ = 1200 μL min^{-1}, corresponding to $\beta = 3.4 \times 10^{-8}$ Pa^{-1} according to Equation (2), which was within the range of compressibility for PDMS materials.[18] This value of β was used to compare model predictions for the HB fluid

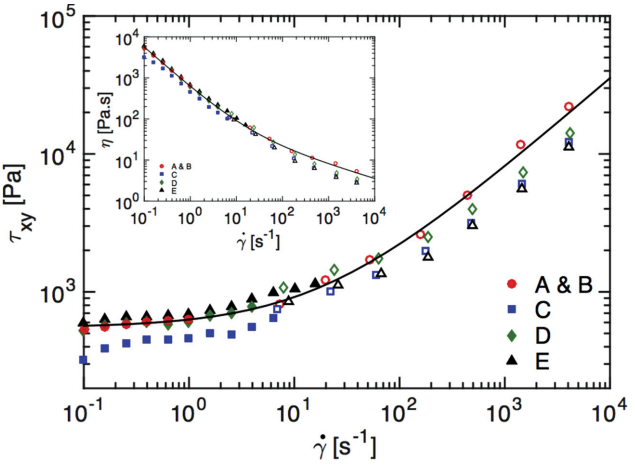

Figure 1. Rheological flow curves of the PDMS ink formulations used in this work. The filled symbols correspond to data taken on the rotational rheometer. The hollow symbols indicate data taken using a capillary rheometer. Both the Bagely correction and the Weissenberg–Rabinowitsch correction were applied to the capillary data. The black solid line is the fit of the Herschel–Bulkley model to formulations A and B.

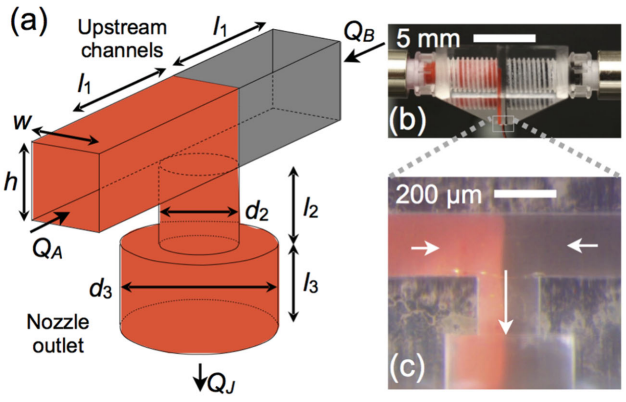

Figure 2. Multimaterial microfluidic printhead. a) Schematic illustration of the nozzle outlet with dimensions. b) Two independently actuated syringe pumps controlled the flow of each material through the nozzle. Red and black PDMS liquids were fed into the nozzle from the syringes and exited from the outlet. c) Close-up view of the microfluidic printhead.

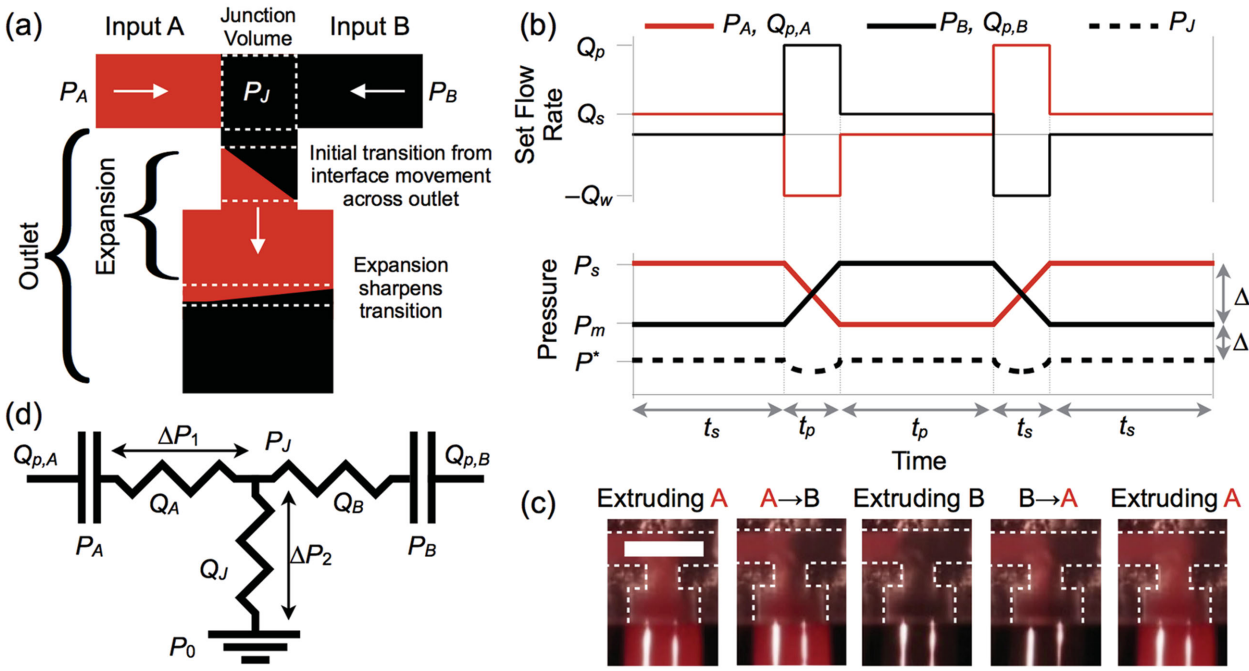

Figure 3. Principle of nozzle operation. a) Materials A and B entered the nozzle and met in a junction of small volume, ≈10 nL. As the pumps induced a transition from extruding A to extruding B, a mixture of A and B flowed into the outlet. The length of this initial transition region was determined by the motion of the interface between the materials across the outlet opening. Expanding the diameter of the outlet further sharpened the transition. b) Microscopy images of the different states of the nozzle during operation. White lines have been added to the images to highlight the edges of the microchannels. c) Plots of the volumetric flow rates set in the syringe pumps and corresponding pressures in the nozzle, which directly drove the transition between materials. The scale-bar indicates 400 μm. d) Schematic illustration of the fluid flow model.

against the experimentally measured transition length and standard deviation in filament width (Figure 4c,d). For pulse values between $1200 < Q_P < 1600$ μL min^{-1} the transition length continued to decrease with increasing Q_p, but the variation in the filament width increased due to larger fluctuations in the junction pressure during the transition process. The transition length reached a minimum of approximately 520 μm at Q_P = 1600 μL min^{-1}. At higher values of $Q_P > 1600$ μL min^{-1}, the transition length and the width variation increased with Q_p. This trend may have been caused by sufficiently large suction pressures during ink withdrawal, causing partial retraction of the filament into the syringe, as well as limitations in the pump accuracy and backlash between the syringe plunger and pump ram. To achieve sharp transitions, the pulse value Q_P = 1600 μL min^{-1} was used as a starting point for printing with PDMS inks (C–E).

To demonstrate multimaterial 3D printing of viscoelastic inks, we created 1D, 2D, and 3D architectures composed of elastomeric inks of varying composition and mechanical properties (**Figure 5**a). First, we printed 1D filaments with small alternating bands present along the printed filament to demonstrate repeated switching between two viscoelastic inks on the length scale of the filament diameter. Next, we printed a 2D structure containing segments of varying lengths to form the letter H. We then created 3D periodic structures in which material transitions occurred in the gaps spanning across orthogonal filaments in the underlying layers. As a final demonstration, we patterned highly integrated 3D architectures composed of elastomeric materials with different mechanical stiffness (Figure 5b). Specifically, alternating bands of different inks were interdigitated in patterns to form printed matrices that exhibited different necking behavior. These initial demonstrations highlight our ability to programmably control the local compositional and mechanical properties within 3D printed objects.

In summary, we have demonstrated multimaterial 3D printing using microfluidic printheads specifically optimized for patterning viscoelastic inks. 3D architectures are printed with sharp transitions between different materials from a single nozzle in a controlled and repeatable manner. We also developed an analytical model of viscoelastic ink flow, from which scaling relationships are derived that enable printhead optimization. Using these novel microfluidic devices, multiple 3D architectures are patterned with programmable compositional and mechanical property gradients over length scales below the characteristic nozzle dimensions. The ability to rapidly switch between multiple inks within a single nozzle printhead not only greatly simplifies tool path planning, but opens new opportunities for the programmable assembly of functional matter.

Experimental Section

Elastomeric Inks: Each ink was prepared by adding one component at a time, proceeding from left to right in Table 1. After each addition, the inks were mixed in a planetary centrifugal mixer (Thinky Mixer) at 2000 rpm for 180 s followed by 30 s of centrifugation. Inks A and B were mixed with 4 μL of QD suspended in toluene per gram of PDMS. Inks C and D were designed to print structures that could be cured, using a 1:10 ratio by mass of catalyst to base. Hexane served as a rheological

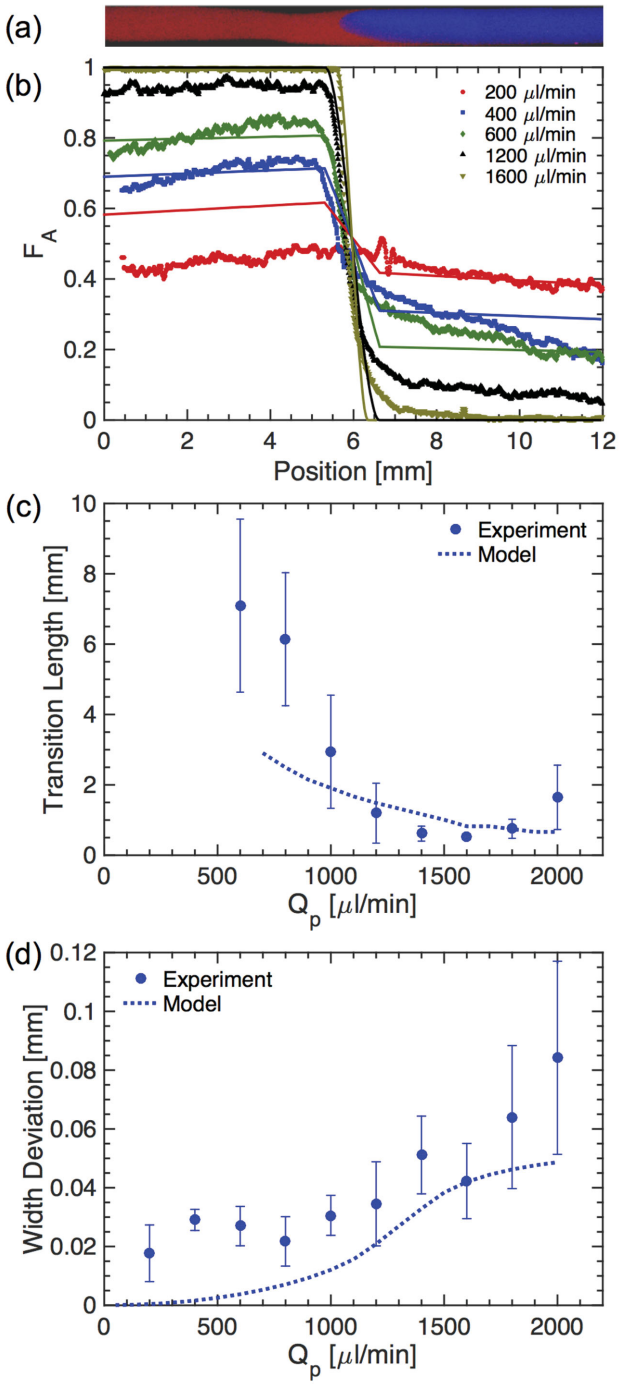

Figure 4. Impact of printing pulse strength on print quality for Q_s = 20 μL min^{-1}. a) Example printed filament laden with QD at Q_p = 1600 μL min^{-1}. The scale of the image is consistent with the abscissa of b) representative intensity profiles along the filament length over the range of pulses and corresponding profiles predicted with the model for $\beta = 3.4 \times 10^{-8}$ Pa^{-1}. c) Transition length and d) standard deviation in filament width over the range of pulses tested. In all cases $Q_w = Q_p - Q_s$.

modifier to lower the viscosity and evaporated quickly upon printing. Ink C contained red pigment. Finally, Ink E contained a catalyst to base ratio of 1:30, yielding a more compliant elastomeric matrix than those with a 1:10 ratio.

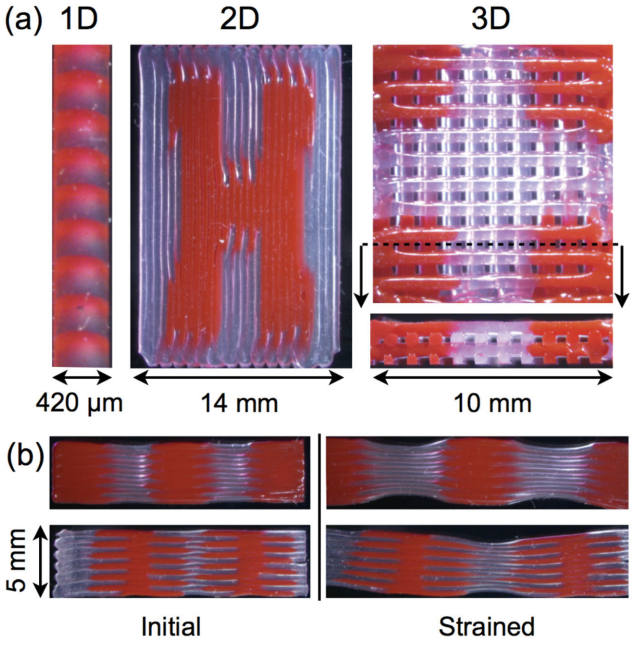

Figure 5. Printed multimaterial structures. a) Image of a 1D extruded filament containing alternating bands of clear and red PDMS with a width of 420 μm. Image of a 2D "H" pattern printed by switching materials. The print pattern consisted of vertical passes and the total width is 14 mm. A 3D four-layer log pile structure with a 1 mm center-to-center spacing of the filaments. An image of a cross section is displayed below it. b) Ribbons of alternating bands of different PDMS materials with different elastic moduli. The ribbons are initially 5 mm in width. Two degrees of interdigitation of the materials result in two different necking behaviors.

Ink Rheology: The ink viscosity was measured at $\dot{\gamma} \leqslant 1 s^{-1}$ using a 40 mm, 2° cone-and-plate on a stress-controlled rotational rheometer (AR2000ex, TA Instruments). At higher shear rates $1 \leqslant \dot{\gamma} \leqslant 1000 s^{-1}$, the ink rheology was measured using a custom-built capillary rheometer. This system consisted of a syringe pump (PHD Ultra, Harvard Apparatus), a 1.0 mL glass Luer lock syringe (Hamilton Gastight), a diaphragm pressure transducer (PX44E0–1KGI, Omega Engineering) and disposable Luer lock needle tips (Norsdon EFD). Capillaries with inner radius R = 514 μm lengths from L = 12.9 mm, 25.4 mm, and 38.3 mm were used. The total pressure drop ΔP_{tot} across the transducer housing and capillary was measured over a range of imposed flow rates. These measurements were repeated using capillaries of the same diameter, but increasing lengths, and the Bagely correction was applied to determine the actual pressure drop across the capillary, ΔP_{cap}. These values were then related to the wall shear stress by $\tau_w = \frac{1}{2}\frac{R}{L}\Delta P_{cap}$. The Weissenberg–Rabinowitsch correction was applied to account for shear-thinning and to determine the true wall shear rate[19] using:

$$\dot{\gamma}_t = \frac{\dot{\gamma}_a}{3}\left[2 + \frac{d\ln\dot{\gamma}_a}{d\ln\tau_w}\right] \quad (3)$$

where $\dot{\gamma}_a = \frac{4}{\pi}\frac{Q}{R^3}$ is the wall shear rate of a Newtonian fluid corresponding to the volumetric flow rate Q. Finally, a third order polynomial was fitted to five consecutive data points to numerically determine the local differential correction term for each data point.

Microfluidic Printheads: The printheads were machined from acrylic (McMaster Carr) in four pieces using a CNC-mill (Wabeco). Two pieces formed the microchannels and the other two formed the tapped inlets for the inks. Polished (Buelar EcoMet250) surfaces were solvent-welded together by soaking the surfaces in acetone for one minute then pressing them together. Fine features were preserved during solvent-welding by

infilling them with wax prior to solvent welding. The outlet was machined into the printhead after all four pieces were solvent-welded together. The nozzle body was then machined down and polished to remove excess materials and Leur lock adapters were screwed into the inlets. Finally, the wax was removed from the microchannels.

Modeling Fluid Flow: To model fluid flow through the microfluidic printhead, we first calculated the Reynolds number given by $Re = \rho U d_2 / \eta(\dot{\gamma})$, where ρ is the density of the fluid, $U = Q / \frac{\pi}{4} d_2^2$ is the mean velocity in the narrow section of the printhead, and $\eta(\dot{\gamma})$ is the rate dependent viscosity described by the HB model at the characteristic shear rate $\dot{\gamma} = U / d_2$ in the flow through the nozzle. Even at the highest flow rates $Re < 10^{-5}$, so the ink flow was laminar.

The governing equations for the evolution of the pressure in each syringe were determined from a mass balance on each syringe (see the Supporting Information):

$$V_A \beta \frac{dP_A}{dt} = Q_{p,A}(t) - Q_A(t) \tag{4}$$

$$V_B \beta \frac{dP_B}{dt} = Q_{p,B}(t) - Q_B(t) \tag{5}$$

where Q_A and Q_B are the net volumetric flow rates of material exiting each syringe. The syringe volumes were assumed to be equal ($V_A = V_B = V$) and were approximated as constant in time, since very small volumes of ink were printed compared to the syringe volume. Density changes in the nozzle junction were neglected, and the flow rate through the nozzle was determined from a mass balance on the junction:

$$Q_J(t) = Q_A(t) + Q_B(t) \tag{6}$$

The relationship between pressure drop ΔP_i and net volumetric flow rate Q_i through any channel was determined by the equation for steady flow of a HB fluid through a cylindrical pipe with radius r_i and length l_i:

$$Q_i = \pi r_i^3 \left(\frac{\sigma_Y}{K}\right)^m \frac{1}{(m+1)} \frac{\alpha^{m+1}}{(1-\alpha)^m} \left[1 - \frac{2\alpha}{(m+2)} + \frac{2\alpha^2}{(m+2)(m+3)}\right] \tag{7}$$

where $m \equiv 1/n$, $\alpha \equiv 1 - \tau_Y / \tau_W$, $\tau_W = \frac{1}{2} \frac{r_i}{l_i} \Delta P_i$. For Q_A and Q_B, $r_i = \frac{1}{2} d_1$, $l_i = l_1$, and $\Delta P_i = P_i - P_J$, while for Q_J, $r_i = \frac{1}{2} d_2$, $l_i = l_2$ and $\Delta P_i = P_J - P_0$ where $P_0 = 0$.

Equation (4)–(7) yield a system of coupled differential equations to determine the evolution of the pressures and flow rates in the nozzle. During the start up process, $Q_A = Q_B = \frac{1}{2} Q_s$, hence the initial conditions for pressures P_A, P_B, and P_J were determined by implicitly solving Equation (7) for these imposed flow rates. For Newtonian materials with the same viscosity, μ, Equation (7) becomes $Q_i = \frac{\pi r_i^4}{8 \mu l_i} \Delta P_i$, for which Equation (4) and (5) are linear and can be solved exactly (see the Supporting Information). However, for HB materials, Equation (4) and (5) are non-linear, but can be approximated using a first order Maclaurin series in time t to determine the evolution of the pressure profile:

$$P_i(t + \Delta t) \approx P_i(t) + \frac{\Delta t}{V\beta}\left(Q_{p,i}(t) - Q_i(t)\right) \tag{8}$$

where Δt is the elapsed time of either the pulse $\Delta t = t_p = 0.5$ s or the steady extrusion $\Delta t = t_s = 2$ s. This equation was sequentially evolved from the initial conditions until the long-term oscillatory state was attained (Figure 3c and the Supporting Information).

Multimaterial 3D Printing: Inks (3 mL) were loaded into the syringes and then centrifuged in custom holders at 3000 RPM (IEC Centra CL2, Thermo Scientific) for 1 h. Hexane was then pulled into each syringe and quickly expelled to assist with removal of air at the exit of the syringe. Inks were printed through the microfluidic printhead using two opposed syringe pumps (PHD Ultra, Harvard Apparatus).

A confocal microscope (LSM710, Zeiss) was used to image the printed filaments. A 7 × 7 array of *z*-stacks is generated using a commercial stitching algorithm (Imaris 7.6.4, Bitplane Scientific Software) from Δz = 9 μm increments. The intensity of each image was rescaled to compensate for the minimal level of speckling caused by QD aggregates in the PDMS. The slices were then summed and scaled to generate the final images, which were analyzed using Matlab (MathWorks) to determine the transition length and variation in filament width. This analysis is similar to the procedure for identifying edge sharpness according to the ISO-13660 protocols.[20] Line edges were defined as the point from the top and bottom edge of the image for which the signal intensity was above the background noise for at least five consecutive pixels.

Since the printing speed was held constant, a large value of $Q_p >> Q_s$ was important for purging the finite volume of the previous material in the nozzle junction as quickly as possible to maintain abrupt transitions in the printed structure. There were, however, practical limitations on the upper bound of the pulse strength that could be imposed. First, the derivation of Equation (2) assumes that the transient pressure profile is purely due to material compression. Mechanical backlash in the syringe pump, syringe or nozzle, or the connections between these elements may also influence the pressure during the transition. Any air bubbles in the ink can strongly affect system compressibility. A further source of error is related to a limited synchronization of the two pumps, defined by being Δt_{sync} out of synchronization. This error arose at the beginning and ending of each transition when, for a short time, only one pump was running at the full pulse strength. The amount of ink pumped or not pumped during the beginning or end of the transition is given by $Q_p \Delta t_{sync}$. These complicating factors are dependent on the ink composition, loading, and setup of the printing system. Thus, Equation (2), though instructive, was only qualitatively valid for this system, and calibration was required for each material.

Supporting Information

Supporting Information is available from the Wiley Online Library or from the author.

Acknowledgements

J.O.H. and T.J.O. contributed equally to this work. This work was supported as part of the Joint Center for Energy Storage Research, an Energy Innovation Hub funded by the U.S. Department of Energy, Office of Science, Basic Energy Sciences. J.O.H. and T.J.O. acknowledge the IC Postdoctoral Research Fellowship Program for support. The authors thank K. Homan and L. Sanders for their experimental assistance, J. Muth for useful discussions, and W. Bai for creation of the cover art material.

Received: January 15, 2015
Revised: March 15, 2015
Published online: April 17, 2015

[1] J. E. Smay, J. Cesarano, J. A. Lewis, *Langmuir* **2002**, *18*, 5429.
[2] K. Sun, T.-S. Wei, B. Y. Ahn, J. Y. Seo, S. J. Dillon, J. A. Lewis, *Adv. Mater.* **2013**, *25*, 4539.
[3] B. Y. Ahn, E. B. Duoss, M. J. Motala, X. Guo, S. Park, Y. Xiong, J. Yoon, R. G. Nuzzo, J. A. Rogers, J. A. Lewis, *Science* **2009**, *323*, 1590.

[4] J. J. Adams, E. B. Duoss, T. F. Malkowski, M. J. Motala, B. Y. Ahn, R. G. Nuzzo, J. T. Bernhard, J. A. Lewis, *Adv. Mater.* **2011**, *23*, 1335.
[5] G. M. Gratson, M. Xu, J. A. Lewis, *Nature* **2004**, *428*, 386.
[6] R. A. Barry, R. F. Shepherd, J. N. Hanson, R. G. Nuzzo, P. Wiltzius, J. A. Lewis, *Adv. Mater.* **2009**, *21*, 2407.
[7] J. N. H. Shepherd, S. T. Parker, R. F. Shepherd, M. U. Gillette, J. A. Lewis, R. G. Nuzzo, *Adv. Funct. Mater.* **2011**, *21*, 47.
[8] B. G. Compton, J. A. Lewis, *Adv. Mater.* **2014**, *26*, 6043.
[9] D. B. Kolesky, R. L. Truby, A. S. Gladman, T. A. Busbee, K. A. Homan, J. A. Lewis, *Adv. Mater.* **2014**, *26*, 3124.
[10] J. T. Muth, D. M. Vogt, R. L. Truby, Y. Menguc, D. B. Kolesky, R. J. Wood, J. A. Lewis, *Adv. Mater.* **2014**, *26*, 6307.
[11] C. J. Hansen, R. Saksena, D. B. Kolesky, J. J. Vericella, S. J. Kranz, G. P. Muldowney, K. T. Christensen, J. A. Lewis, *Adv. Mater.* **2012**, *25*, 96.
[12] D. J. Lorang, D. Tanaka, C. M. Spadaccini, K. A. Rose, N. J. Cherepy, J. A. Lewis, *Adv. Mater.* **2011**, *23*, 5055.
[13] N. Oxman, *Virtual Phys. Prototyp.* **2011**, *6*, 3.
[14] B. K. Deuser, L. Tang, R. G. Landers, M. C. Leu, G. E. Hilmas, *J. Manuf. Sci. Eng.* **2013**, *135*, 041015.
[15] R. B. Bird, R. C. Armstrong, O. Hassager, *Dynamics of Polymer Liquids*, Vol. *1*, 2nd ed., John Wiley & Sons, New York, **1987**.
[16] P. Coussot, *J. Fluid Mech.* **1999**, *380*, 363.
[17] H. A. Stone, A. D. Stroock, A. Ajdari, *Annu. Rev. Fluid Mech.* **2004**, *36*, 381.
[18] Y. A. Fakhreddine, P. Zoller, *J. App. Poly. Sci.* **1990**, *41*, 1087.
[19] C. W. Macosko, *Rheology Principles, Measurements and Applications*, Wiley-VCH, Weinheim, Germany, **1994**.
[20] J. C. Briggs, D. J. Forrest, A. H. Klein, M. K. Tse, in *NIP Digital Fabrication Conference*, Society for Imaging Science and Technology, Orlando, FL, USA, **1999**.